Aldi Fahli Muzaqih[1], *Muhamad Imam Firdaus*[2], *Ristiyanto Adiputra*[3*], *Aditya Rio Prabowo*[1**], *Sharath Srinivasamurthy*[4], *Adnan Sandy Dwi Marta*[5]

SANDWICH COMPOSITE UTILISATION FOR FLOATING OSCILLATING WATER COLUMN STRUCTURE: PRELIMINARY ANALYSIS UNDER IMPULSE LOADS

UPOTREBA SENDVIČ KOMPOZITA ZA PLUTAJUĆU OSCILUJUĆU KONSTRUKCIJU VODENOG STUBA: PRELIMINARNA ANALIZA SA IMPULSNIM OPTEREĆENJIMA

Originalni naučni rad / Original scientific paper
Rad primljen / Paper received: 23.02.2026
https://doi.org/10.69644/ivk-2026-siA-0045

Adresa autora / Author's address:
[1]) Department of Mechanical Engineering, Universitas Sebelas Maret, Surakarta, Indonesia **email: aditya@ft.uns.ac.id ,
A.F. Muzaqih https://orcid.org/0009-0001-2023-9284 ;
A.R. Prabowo https://orcid.org/0000-0001-5217-5943
[2]) Banten Merchant Polytechnic, Banten, Indonesia
M.I. Firdaus https://orcid.org/0000-0003-0539-0661
[3]) Research Center for Hydrodynamics Technology, National Research and Innovation Agency, South Tangerang, Indonesia
*email: ristiyanto.adiputra@brin.go.id ,
R. Adiputra https://orcid.org/0000-0003-3630-9432
[4]) Institute of Ocean Energy, Saga University, Saga, Japan
S. Srinivasamurthy https://orcid.org/0000-0001-9915-6301
[5]) Fluid Mechanics Laboratory, National Research and Innovation Agency, South Tangerang, Indonesia
A.S.D. Marta https://orcid.org/0009-0006-0768-0709

Keywords
- blast load
- energy absorption
- finite element analysis
- ultimate capacity

Abstract

Composite materials have promising potential for renewable energy applications, such as the structure for the Oscillating Water Column (OWC). As OWC structures are continuously subjected to impulsive wave loads, understanding their structural response is crucial for ensuring reliability and safety. This study investigates the structural strength and integrity of composite sandwich panels under impulsive loading using the Finite Element Method (FEM) implemented in ABAQUS® Simulia with an adapted Underwater Shock Loading Simulator (USLS) model. Various configurations are evaluated by combining different facesheet materials, core types, and adhesive systems. The results show that PVC foam cores provide superior stiffness with displacements as low as 1.3 mm. In terms of impulse transmission, Nomex honeycomb cores exhibit the best damping performance, reducing reaction forces to approximately 3.5 kN. Energy absorption analysis reveals that the carbon-SAN foam-polyurethane configuration achieves the highest absorbed energy of 22 kJ.

Ključne reči
- eksplozivno opterećenje
- apsorpcija energije
- analiza konačnim elementima
- maksimalni kapacitet

Izvod

Kompozitni materijali imaju potencijal u primeni obnovljivih izvora energije, kao što je konstrukcija za oscilujući vodeni stub (OWC). Pošto su OWC konstrukcije kontinuirano izložene talasnim opterećenjima, razumevanje njihovog konstrukcionog odgovora je ključno za pouzdanost i bezbednost. Ova studija istražuje čvrstoću i integritet kompozitnih sendvič panel konstrukcija pod impulsnim opterećenjem korišćenjem metode konačnih elemenata (FEM) implementirane u ABAQUS® Simulia sa prilagođenim modelom simulatora podvodnog udarnog opterećenja (USLS). Različite konfiguracije su procenjene kombinovanjem različitih materijala oklopnog sloja, tipova jezgara i sistema lepljenja. Rezultati pokazuju da jezgra od PVC pene pružaju superiornu krutost sa pomeranjima i do 1,3 mm. U smislu prenosa impulsa, jezgra od Nomex saća pokazuju najbolje performanse prigušenja, smanjujući sile reakcije na približno 3,5 kN. Analiza apsorpcije energije otkriva da konfiguracija karbon-SAN pena-poliuretan postiže najveću apsorbovanu energiju od 22 kJ.

INTRODUCTION

The increasing global energy demand underscores the importance of developing sustainable renewable energy technologies /1-3/. Among the available alternatives, the utilisation of ocean wave energy through the Oscillating Water Column (OWC) system represents a promising renewable energy option with significant potential for both coastal and offshore applications. The OWC structure operates by using the oscillation of a water column induced by ocean waves to drive an air turbine, thereby generating electrical energy in a continuous manner /4/. During operation, OWC structures are continuously exposed to dynamic and impulsive wave loads, including extreme wave pressures and transient loads caused by varying sea conditions. These loads may induce high stresses, local deformation, and structural damage, making structural strength and integrity key factors in ensuring the reliability and safety of the OWC structure.

Conventionally, OWC structures, particularly floating types, are designed using metallic materials such as steel and aluminium, /5/. Although these materials provide good structural strength, they also have disadvantages, including relatively high weight, susceptibility to corrosion, and high installation and maintenance costs in marine environments /6/. These limitations have increased interest in composite materials as alternative structural materials for marine and ocean energy systems due to their high strength-to-weight ratio and good corrosion resistance, /7, 8/.

One widely developed type of composite material is the sandwich composite which consists of a facesheet that resists bending stresses and a core layer that increases stiffness and absorbs impact loads, with both layers bonded using adhesive materials /9, 10/. The structural efficiency and energy-absorption capabilities of sandwich composites have encouraged their application in various engineering structures, including marine and offshore systems /11/. However, studies that specifically investigate the application of sandwich composites in OWC structures remain limited. Therefore, further investigation is required to evaluate the response and resistance of sandwich composites to impulsive loads acting on OWC structures, particularly under extreme wave conditions.

Previous research on OWC structures has mainly focused on hydrodynamic analysis and the identification of stress distribution and critical structural regions under wave loading /12-14/. One of the significant load types acting on OWC structures is impulsive loading caused by extreme ocean waves. To investigate structural responses under impulsive loading, several previous studies have employed USLS approach. Avachat et al. /15/ examined the response of CFRP and GFRP laminates under impulsive loading using the USLS method. Feng et al. /16/ studied the influence of foam core type and thickness on the impulsive response of sandwich panels. Wei and Rong /17/ analysed the behaviour of CFRP laminates under impulsive loads. These studies indicate that the USLS method is a promising approach for representing impulsive loading, yet investigations covering multiple sandwich composite configurations remain limited.

Based on this background, the present study proposes investigating the dynamic response of sandwich composite panels in oscillating water column structures under impulsive loading in marine environments using an USLS approach modelled through the finite element method (FEM). The analysis evaluates maximum capacity, stress distribution, and energy absorption in sandwich composite structures with various face-sheet materials, core types, and adhesive materials. The findings of this study are expected to provide a basis for developing lightweight, strong, and impulsive-load-resistant sandwich composite-based OWC structures for marine applications.

METHODS

Impulsive load simulation

In this study, the wave impacts on the OWC structure are represented as seawater impulsive loads that are numerically modelled using an USLS by applying controlled impulsive loading to test specimens. The numeric USLS model is duplicated from a previous experimental study by He et al. /18/ as illustrated in Fig. 1.

The detailed schematic simulation is available in /16/. In principle, the impulsive load is generated by the impact between a flyer and a piston, which triggers the formation of a pressure wave within the fluid. This pressure wave propagates and reflects at the interface between the piston and the fluid domain, resulting in an equivalent shock wave. As the shock wave travels through the target chamber, its magnitude decays exponentially before finally reaching the test specimen.

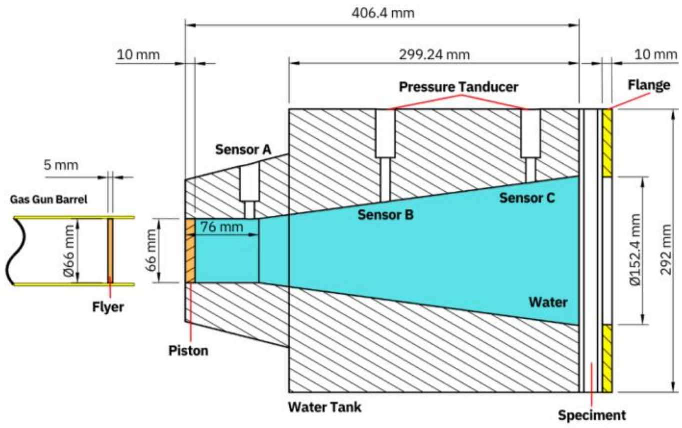

Figure 1. Schematic underwater shock loading simulator, /16/.

In a floating OWC structure, impulsive loading represents extreme wave impact events caused by steep or breaking waves that generate very high pressures within a short duration characterised by a rapid pressure rise and brief loading time; therefore, this impulsive load is applied as a conservative approach to evaluate the maximum strength and energy absorption capacity of the sandwich composite panel under extreme wave impact conditions.

According to Taylor's analysis, the shock wave pressure generated by an underwater explosion can be expressed as:

$$p(t) = p_0 \exp\left(-\frac{t}{t_0}\right), \qquad (1)$$

where: p_0 represents peak pressure; and θ is decay time. The flyer mass per unit area determines both parameters m_f and initial impact velocity v_0. Therefore, the peak pressure can be expressed as:

$$p_0 = \rho_w c_w v_0 \,. \qquad (2)$$

Meanwhile, the decay time of the pressure wave is given by:

$$\theta = \frac{m_f}{\rho_w c_w} \,. \qquad (3)$$

The total impulse generated by the shock wave is defined as:

$$I_0 = \int_0^t p(t)dt = p_0 t_0 \,. \qquad (4)$$

To compare the responses of various sandwich structures under different impulsive loading conditions, the concept of dimensionless impulse is used /3/, which is defined as:

$$\hat{I} = \frac{I_0}{\bar{M}\sqrt{\sigma_y/\rho}} \,, \qquad (5)$$

where: $\bar{M}$ is mass per unit area; σ_y is yield stress of the material; and ρ is the target material density.

Finite element simulation

The overall research workflow is illustrated in Fig. 2. This study begins with a literature review examining relevant theories, numerical methods, and prior studies. Based on this theoretical foundation, the numerical simulation is then developed using ABAQUS® Simulia, applying the FEM /19/ and Coupled Eulerian-Lagrangian (CEL) method to model the interaction between solid structures and the fluid domain.

To implement this numerical framework, the research is initiated by modelling the USLS geometry based on predefined dimensions, defining material properties, specifying interactions between parts, and applying loading and boundary conditions. Meshing process is subsequently carried out along with a mesh convergence analysis to determine the optimal element size and ensure accurate and stable simulation results.

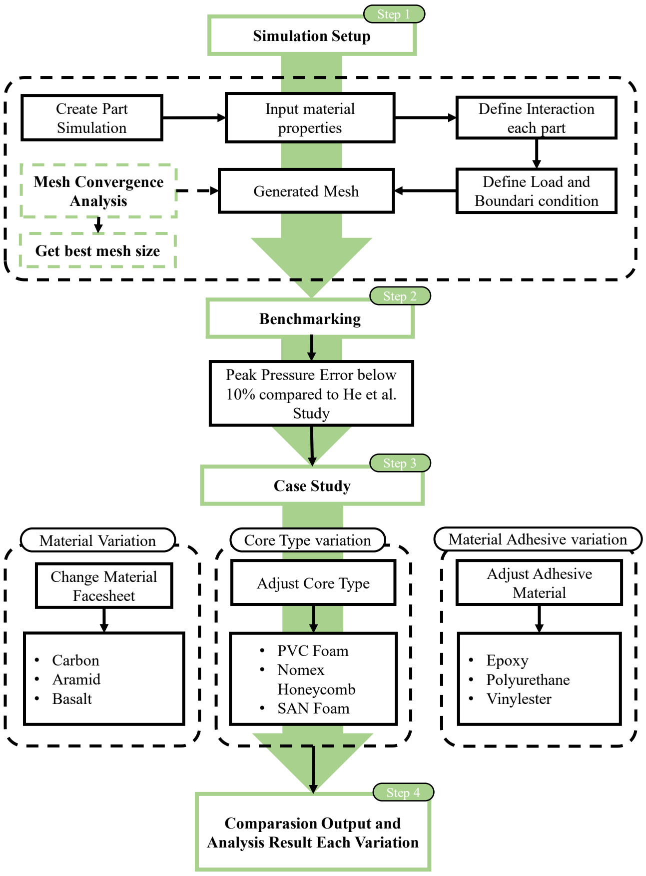

Figure 2. Research flow of the current study.

The developed simulation model is validated through benchmarking against the study conducted by He et al. /18/, with a target error of less than 10 %. After the model is validated, further analyses are performed by varying several parameters, including the facesheet material, core material type, and adhesive material. The results of each variation are compared and analysed to assess the influence of each parameter on the structural response, yielding the study's main conclusions.

The materials defined in this study include a fluid domain modelled using an Equation of State (EOS), steel 4340 used for the water tank and flange, steel 4140 used for the piston and flyer, and the specimen material under investigation. Material properties for both the fluid domain and the solid domain applied in the simulation are presented in Tables 1 and 2.

Table 1. Material properties for steel 4340 and steel 4140 /18/.

Materials	Density ρ (kg·m^{-3})	Young modulus E (GPa)	Poisson ratio ν	Yield stress σ_y (MPa)
steel 4340	7850	205	0.29	470
steel 4140	7850	205	0.29	1000

Table 2. Material properties of water /20/.

Density ρ (kg·m^{-3})	Speed of sound c_0 (m·s^{-1})	Gamma γ
1000	1482	0.1

The test specimen used for the validation process consists of aluminium 3004 as the facesheet material and aluminium foam as the core material. The facesheet has a thickness of 0.4 mm, while the core has a thickness of 14 mm. The material properties of aluminium 3004 and aluminium foam core are presented in Table 3, and the failure criterion applied to the facesheet material is the ductile damage model with Johnson-Cook parameters. Material properties are defined under dry conditions, and the effects of seawater immersion or long-term water absorption on material degradation are not considered.

Table 3. Material properties of Al 3004 and Al foam, /20/.

Parameters	Symbol	Units	Al 3004	Al foam
Density	ρ	kg/m^3	2700	300
Young's modulus	E	GPa	70	5
Poisson's ratio	ν		0.3	0.3
Yield stress (Johnson-Cook)	A	MPa	125	125
Hardening modulus (Johnson-Cook)	B	MPa	282.5	282.5
Strain rate sensitivity Johnson-Cook	C	-	0.0832	0.084
Strain hardening exponent	N	-	0.44	0.44
Thermal softening exponent	M	-	2.09	2.09

Boundary conditions are applied to represent the physical constraints of the system during simulation. In this study, an encastre boundary condition [U1, U2, U3, UR1, UR2, UR3=0] is imposed on the water tank and flange to ensure that these components remain fully fixed. All solid components are modelled using three-dimensional finite elements of type C3D8R, while the composite structures are represented using shell elements of type S4R (with 4 nodes /21/), and the adhesive layers are modelled using cohesive elements of type COH3D8. Initial mesh sizes for each component are adopted based on the study by He et al. /18/ as the reference model. The meshing process is then performed for each component, with detailed mesh sizes presented in Fig. 3. For the water domain, the mesh size is further evaluated using a mesh convergence analysis to obtain optimal, numerically stable simulation results.

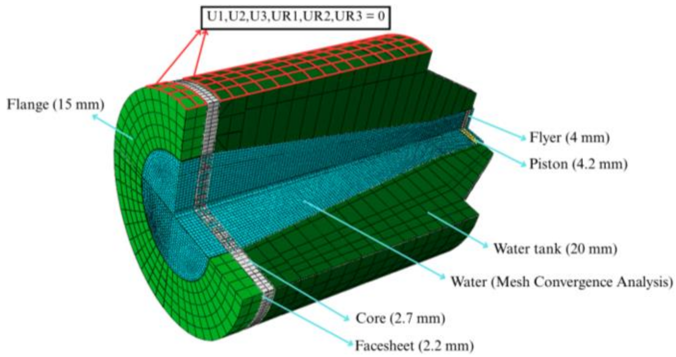

Figure 3. Mesh size for each part and the boundary condition.

Interactions between parts in the simulation are defined using general contact, while the interaction between piston and flyer is modelled using surface-to-surface contact. For the sandwich panel specimen, a tie constraint is applied to bond the facesheet layers of the lamina. The loading condition is defined by applying an initial velocity (v_0) to the flyer, which generates the initial pressure when the flyer impacts the piston. In addition, a gravity acceleration of 9.81 m/s² and a hydrostatic pressure of 101 Pa are applied, primarily in the fluid domain. A predefined field is used to define the Eulerian domain representing water and air.

Parametric case study

Case studies conducted in this research include variations in facesheet materials, core types, and adhesive materials. These parameter variations are systematically designed to analyse the influence of each factor on the structural response and performance. Detailed specifications for each planned case configuration are presented in Table 4.

Table 4. Configurations of the parametric study.

Case code	Parameters		
	Face sheet material	Core type	Adhesive
F1-C1-A1	carbon	PVC foam	epoxy
F1-C1-A2	carbon	PVC foam	polyurethane
F1-C1-A3	carbon	PVC foam	vinyl ester
F1-C2-A1	carbon	Nomex honeycomb	epoxy
F1-C2-A2	carbon	Nomex honeycomb	polyurethane
F1-C2-A3	carbon	Nomex honeycomb	vinyl ester
F1-C3-A1	carbon	SAN foam	epoxy
F1-C3-A2	carbon	SAN foam	polyurethane
F1-C3-A3	carbon	SAN foam	vinyl ester
F2-C1-A1	aramid	PVC foam	epoxy
F2-C1-A2	aramid	PVC foam	polyurethane
F2-C1-A3	aramid	PVC foam	vinyl ester
F2-C2-A1	aramid	Nomex honeycomb	epoxy
F2-C2-A2	aramid	Nomex honeycomb	polyurethane
F2-C2-A3	aramid	Nomex honeycomb	vinyl ester
F2-C3-A1	aramid	SAN foam	epoxy
F2-C3-A2	aramid	SAN foam	polyurethane
F2-C3-A3	aramid	SAN foam	vinyl ester
F3-C1-A1	basalt	PVC foam	epoxy
F3-C1-A2	basalt	PVC foam	polyurethane
F3-C1-A3	basalt	PVC foam	vinyl ester
F3-C2-A1	basalt	Nomex honeycomb	epoxy
F3-C2-A2	basalt	Nomex honeycomb	polyurethane
F3-C2-A3	basalt	Nomex honeycomb	vinyl ester
F3-C3-A1	basalt	SAN foam	epoxy
F3-C3-A2	basalt	SAN foam	polyurethane
F3-C3-A3	basalt	SAN foam	vinyl ester

Facesheet materials considered in this study are composites with high resistance to harsh seawater environments: carbon fibre-reinforced polymer (CFRP), aramid fibre-reinforced polymer (AFRP), and basalt fibre-reinforced polymer (BFRP). Mechanical properties are presented in Table 5. The damage initiation of the composite facesheet is evaluated using the Hashin failure criteria, which distinguishes between fibre and matrix failure modes under tensile and compressive loading conditions, following Eqs.(6)-(9).

$$F_f^t = \left(\frac{\sigma_{11}}{s_{t1}}\right)^2 + \alpha\left(\frac{\sigma_{12}}{s_{s12}}\right)^2 \le 1.0 \quad \text{and} \quad \sigma_{11} \ge 0, \tag{6}$$

$$F_f^c = \left(\frac{\sigma_{11}}{s_{c1}}\right)^2 \le 1.0 \quad \text{and} \quad \sigma_{11} \ge 0, \tag{7}$$

$$F_m^t = \left(\frac{\sigma_{22}}{s_{t2}}\right)^2 + \left(\frac{\sigma_{12}}{s_{s12}}\right)^2 \le 1.0 \quad \text{and} \quad \sigma_{22} \ge 0, \tag{8}$$

$$F_m^c = \left(\frac{\sigma_{22}}{2s_{s23}}\right)^2 + \left[\left(\frac{s_{c2}}{2s_{s23}}\right)^2 - 1\right]\frac{\sigma_{22}}{s_{c2}} + \left(\frac{\sigma_{12}}{s_{s12}}\right)^2 \le 1.0 \quad \text{and} \quad \sigma_{22} \ge 0, \tag{9}$$

where: σ_{11}, σ_{22}, and σ_{12} represent stresses; s_{ti}, s_{ci}, and s_{sij} denote the tensile-, compressive-, and shear strengths, respectively. Parameter α is a coefficient ($0.0 \le \alpha \le 1.0$) associated with shear stress σ_{12}.

Table 5. Material properties: CFRP /15/, AFRP /22/, BFRP /23/.

Parameters	Symbol	Units	CFRP	AFRP	BFRP
Density	ρ	kg·m^{-3}	1580	1400	2700
Poisson ratio	ν	-	0.29	0.4	0.2
Longitudinal tensile modulus	E_{11}	GPa	138	83	37.7
Transverse tensile modulus	E_{22}	GPa	10	7	5.237
Shear modulus	G_{12}, G_{13}	GPa	5.24	2.1	3.07
Longitudinal tensile strength	T_{11}	GPa	2.28	1.377	1.1
Long.compressive strength	C_{11}	MPa	1330	235	750
Transverse tensile strength	T_{22}	MPa	57	18	35
Trans.compressive strength	C_{22}	MPa	228	53	150
Longitudinal shear strength	S_{12}, S_{13}	MPa	71	34	60
Transverse shear strength	S_{23}	MPa	71	34	60

Core materials include PVC foam, Nomex honeycomb, and styrene acrylonitrile (SAN). Core material properties are summarised in Table 6. In addition, the adhesive materials employed in this study are araldite 138 epoxy, Sikaflex-292i polyurethane, and Atlac 580 vinyl ester, with their corresponding mechanical properties listed in Table 7.

Table 6. Core material properties: PVC foam /24/, Nomex honeycomb /25/, SAN foam /26/.

Materials	Density ρ (kg·m^{-3})	Young modulus E (MPa)	Poisson ratio ν
PVC foam HP 200	200	310	0.4
Nomex honeycomb	1400	3400	0.3
SAN foam	103	85	0.3

Table 7. Adhesive material properties: epoxy /15/, polyurethane /27/, vinyl ester /26/.

Parameters	Symbol	Units	Epoxy araldite 138	Polyurethane Sikaflex-292i	Vinyl ester Atlac 580
Density	ρ	kg/m^3	1100	1125	1125
Poisson ratio	ν	-	0.35	0.4	0.37
Tensile modulus	E_n	GPa	2	2.25	3.5
Shear modulus	G_s, G_t	GPa	2	0.821	1.28
Critical normal traction	t_n^0	MPa	50	18	40.618
Critical shear traction	t_s^0, t_t^0	MPa	50	30	40.618

The facesheet is bonded to the core using an adhesive layer modelled as a cohesive element, while the core is modelled using solid elements with a crushable foam material model (see Fig. 4). As for the Nomex honeycomb core, its cell geometry is explicitly modelled according to the configuration shown in Fig. 5.

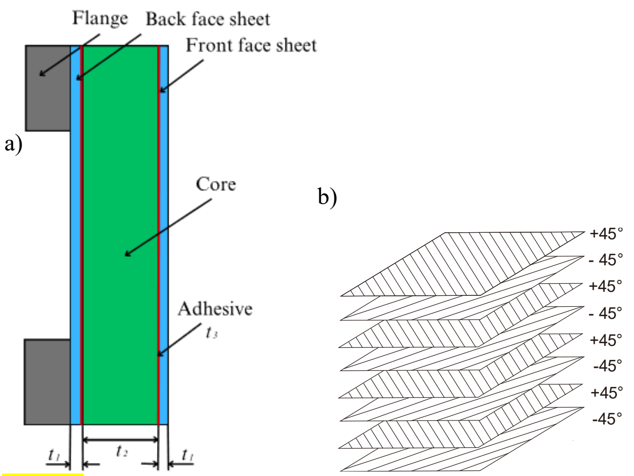

Figure 4. Schematic of the specimen testing model: a) composite sandwich layer configuration; b) fibre orientation in the facesheet.

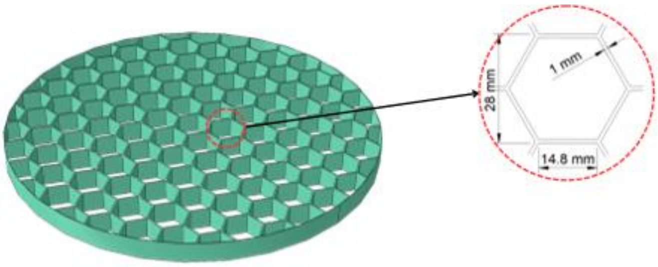

Figure 5. Geometric core honeycomb.

BENCHMARKING STAGE

Mesh convergence

The mesh convergence analysis focuses on the pressure measured in the fluid domain, particularly at sensor B. The mesh size was varied from 12 to 2 mm to evaluate the influence of mesh resolution on the simulation results. The mesh convergence results indicate that measured peak pressure varies with mesh refinement, as shown in Fig. 6.

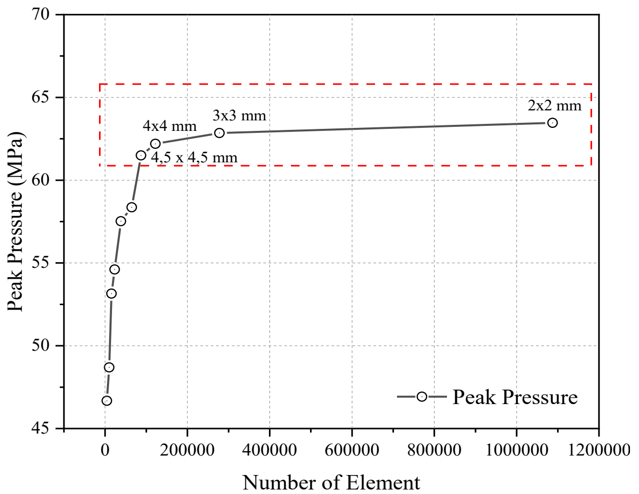

Figure 6. Mesh convergence analysis results.

To assess the convergence level and evaluate the numerical discretisation uncertainty, the Richardson Extrapolation method and the Grid Convergence Index (GCI) are applied. Richardson Extrapolation estimates the asymptotic (grid-independent) solution by assuming that numerical results follow a systematic convergence trend as the mesh is progressively refined. At the same time, the GCI provides a quantitative and conservative measure of the discretisation error between successive mesh refinements. The observed order of convergence, the extrapolated solution, and GCI value are calculated using Eqs.(10), (11), and (12), in respect,

$$p = \frac{\ln\left(\frac{f_3 - f_2}{f_2 - f_1}\right)}{\ln(r)}, \tag{10}$$

$$f_{ext} = f_3 + \frac{f_3 - f_2}{r^p - 1}, \tag{11}$$

$$\mathrm{GCI} = F_s \frac{|f_3 - f_2|}{|f_3|(r^p - 1)}, \tag{12}$$

where: p is order convergence; f_{ext} is Richardson exploration; f_1, f_2, and f_3 represent numerical solutions obtained from the coarse, medium, and fine meshes, in respect; r is grid refinement ratio; and F_s is safety factor (1.25 for a three-grid study). In this study, a GCI value below 2 % is adopted as the convergence criterion.

The three finest mesh sizes are analysed, including 4.5, 3, and 2 mm, with a constant refinement ratio (r = 1.5). The simulation results show that for 4.5 mm mesh with 87210 elements, the measured peak pressure is 61.5 MPa. When the mesh is refined to 3 mm (277760 elements), the pressure increases to 62.85 MPa, and for the 2 mm mesh (1087240 elements), the peak pressure reaches 63.46 MPa.

The results of the GCI calculations are summarised in Table 8. The Richardson value of 63.96 MPa provides an estimated theoretical peak pressure for an extremely fine mesh and shows a consistent convergence trend toward the experimental reference. The GCI for the two meshes (2 and 3 mm) is approximately 2 %, indicating good consistency between them. Based on this convergence behaviour, and considering the balance between accuracy and computational efficiency, the 3 mm mesh is selected as the primary mesh size for the subsequent analyses.

Table 8. Simulation time comparison.

Mesh size	Element	Peak pressure	Relative difference	GCI	Simulation time
4.5 mm	87210	61.5 MPa	-	-	62 Minute
3 mm	277760	62.85 MPa	3.25 %	4.17 %	118 Minute
2 mm	1087240	63.46 MPa	0.96 %	1.4 %	556 Minute

Validation result

Validation is carried out by comparing numerical simulation results with experimental data reported by He et al. /16/. Experimental results show that the highest pressure occurs at Sensor B, with a value of 61.4 MPa at an initial velocity of 135 m/s, indicating the area with the most significant shock-wave response. The total simulation time is set to 1 ms, corresponding to the time required for the shock wave to propagate and dissipate within the fluid domain.

The validation results are presented in Fig. 7. The simulation predicts a peak pressure of 62.3 MPa. In comparison, He et al. /16/ report an experimental peak pressure of 65.1 MPa at the same time. In their simulation, He et al. recorded a peak pressure of 61.4 MPa. A detailed comparison of the validation outcomes is summarised in Table 9. The discrepancies between the results are all below 10 %, indicating good agreement and confirming that the numerical model accurately captures shock-wave behaviour.

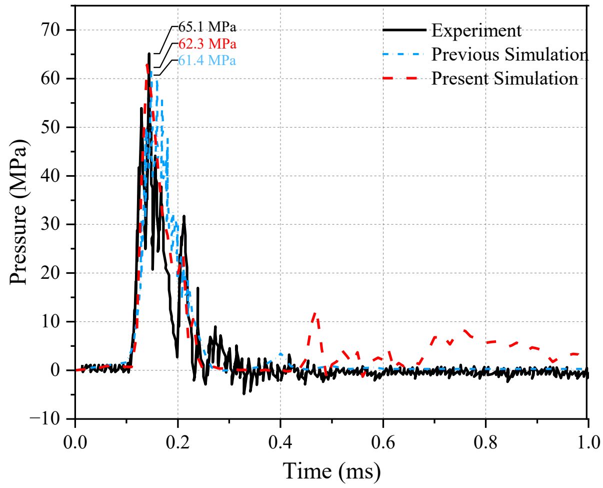

Figure 7. The pressure-time histories in sensor B.

Table 9. Comparison of simulation results with previous research.

Parameter	Experiment	Simulation	Present study	Error exp.	Error sim.
Peak pressure	65.1 MPa	61.4 MPa	62.3 MPa	4.3 %	1.4 %

Pressure fluctuations observed after 0.4 ms are attributed to secondary reflections of residual shock waves within the confined fluid domain of the chamber. These oscillations arise from wave interactions at the chamber boundaries and the piston-fluid interface. Since their magnitude is significantly lower than that of the primary peak pressure, they do not substantially influence the structural response assessment, which is primarily governed by the initial shock peak.

RESULTS AND DISCUSSION

Ultimate capacity

In this study, the ultimate capacity of composite sandwich structures under impulsive loading is evaluated by comparing maximal displacement values. All displacement measurements are consistently taken at the centre point of the composite sandwich panel to ensure uniformity and comparability of the results across different configurations.

Among all variations studied, the highest maximal displacement occurs in the configuration with a basalt facesheet, Nomex honeycomb core, and polyurethane adhesive, with a maximal displacement of 2.26 mm, as shown in Fig. 8. This result indicates that this configuration has the lowest structural stiffness under impulsive loading among the variations.

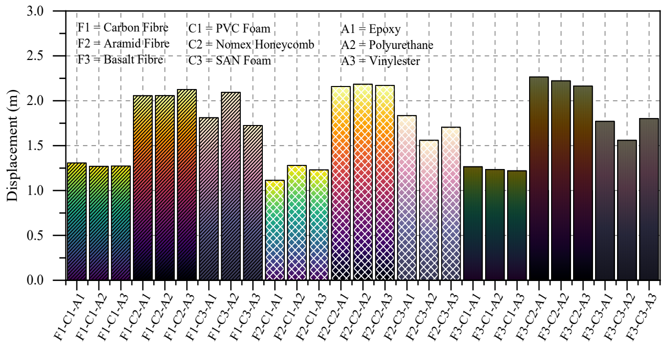

Figure 8. Comparison of maximal displacement in each case.

Based on the observed graph trends, sandwich structures with Nomex honeycomb cores consistently exhibit relatively larger displacements across almost all material variations. This behaviour is attributed to the intrinsic characteristics of honeycomb cores, which have lower effective shear stiffness and higher compliance in the thickness direction. Under impulsive loading, the thin cell walls of the honeycomb tend to undergo shear deformation and local buckling, increasing the global deflection of the sandwich panel.

In contrast, the simulation results show that sandwich structures with PVC foam cores experience smaller displacements. For example, in the configuration with a carbon face sheet and a PVC foam core, the maximal displacement across all adhesive material variations is only around 1.3 mm. This indicates that PVC foam has greater resistance to impulsive loading than honeycomb cores.

Effect of facesheet material

The analysis of facesheet material variations is conducted to evaluate the structure's dynamic response under impulsive loading. Figure 9a shows the relationship between displacement and time, where at 1 ms the carbon facesheet exhibits the highest displacement of 1.3 mm, followed by basalt at 1.25 mm and aramid at 1.1 mm. This indicates that during the initial loading phase, the carbon facesheet tends to produce larger displacements.

However, the trend shown in Fig. 9b indicates that a carbon facesheet does not always yield maximal deflection

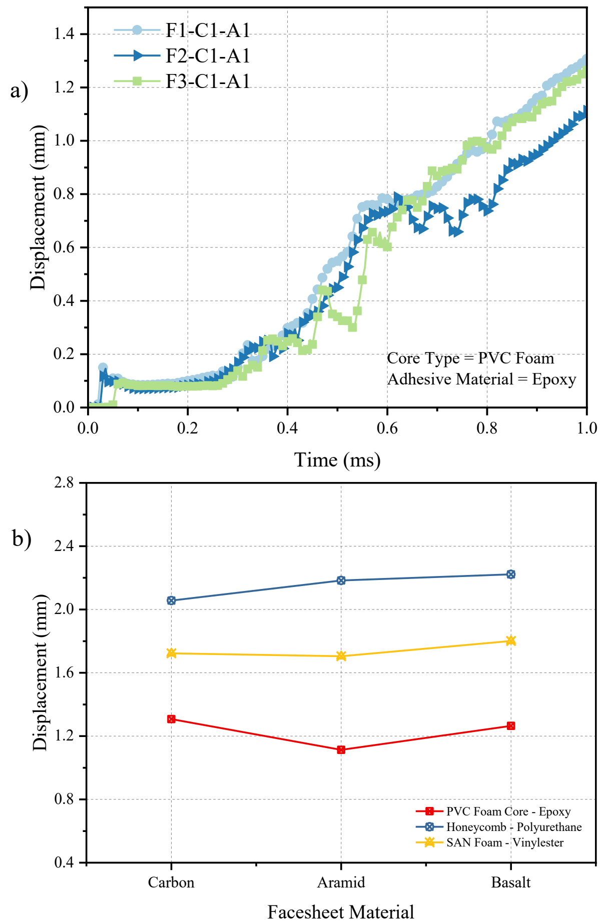

Figure 9. Effect of facesheet material (a) time history of displacement (b) comparison of displacement.

across all configurations. In combinations using SAN foam-vinyl ester and honeycomb-polyurethane cores, the basalt facesheet instead shows the highest displacement. Meanwhile, for honeycomb core configurations, the carbon facesheet exhibits the best structural performance, with the lowest displacement among facesheet materials. This confirms that the interaction between the facesheet, core, and adhesive material strongly influences the deflection response.

Effect of core type

The effect of different core types in this study is clearly illustrated in Fig. 10a, using an aramid facesheet and a polyurethane adhesive in a uniform configuration.

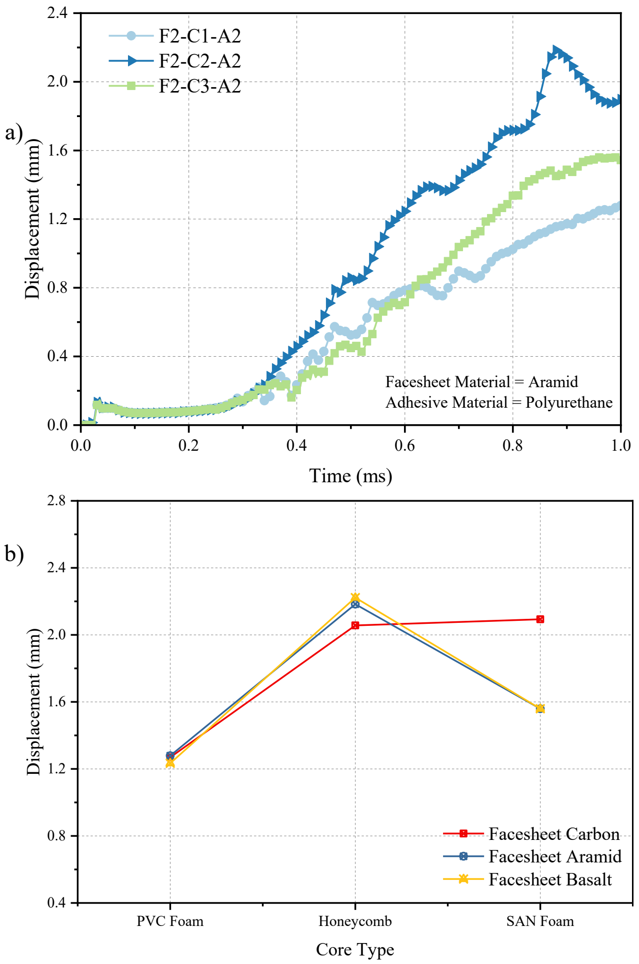

Figure 10. Effect of core type: a) time history of displacement; b) comparison of displacement.

The analysis results show that the honeycomb core produces the largest displacement, followed by SAN foam, while the smallest displacement occurs in PVC foam. In general, the displacement response trends for each core variation exhibit a consistent pattern. However, in the configuration with a carbon facesheet and SAN foam core, relatively larger deformation is observed, which slightly deviates from that observed in other configurations (see Fig. 10b).

Effect of adhesive material

Figure 11a shows that variations in adhesive material have only a limited effect on the sandwich structure's response to impulse loads. In the uniform material configuration with a honeycomb core, the epoxy adhesive yields the highest maximal displacement of 2.26 mm, which decreases to 2.22 mm with polyurethane adhesive, and to 2.16 mm with the vinyl ester adhesive, representing decreases of 1.77 and 4.42 %, respectively. These results indicate that vinyl ester adhesive provides the best performance in resisting impulse loads. However, overall, the effect of the adhesive material is smaller than that of the core type.

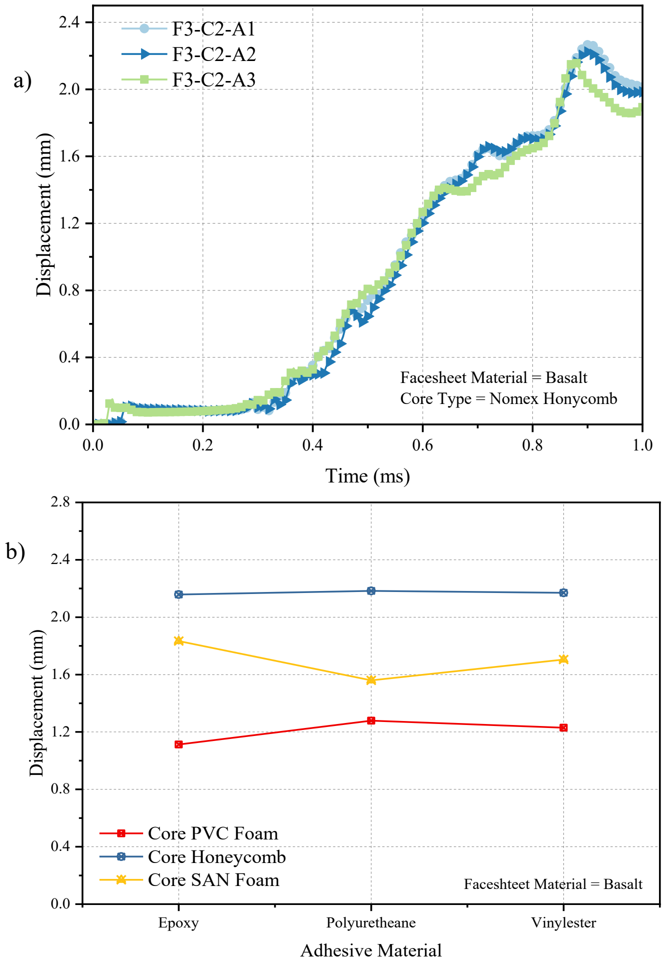

Figure 11. Effect of adhesive material: a) time history displacement facesheet material; b) comparison of displacement.

However, the adhesive performance is still influenced by the configuration of the other materials, as shown in Fig. 11b. In the uniform material configuration with a PVC foam core, the lowest displacement is consistently observed, whereas in the SAN foam core configuration, the minimal displacement is achieved with a polyurethane adhesive. Meanwhile, for the honeycomb core, the maximal displacement values are relatively uniform across all adhesive variations, indicating that the core's mechanical characteristics dominate the structural response more than the adhesive material.

Transmitted impulse

The transmitted impulse is analysed to determine the extent to which the sandwich structure can resist and transmit impulse loads. In this study, the transmitted impulse values are obtained from the reaction force data measured on the specimens, particularly at the flange. The reaction force graphs for all case variations are shown in Fig. 12.

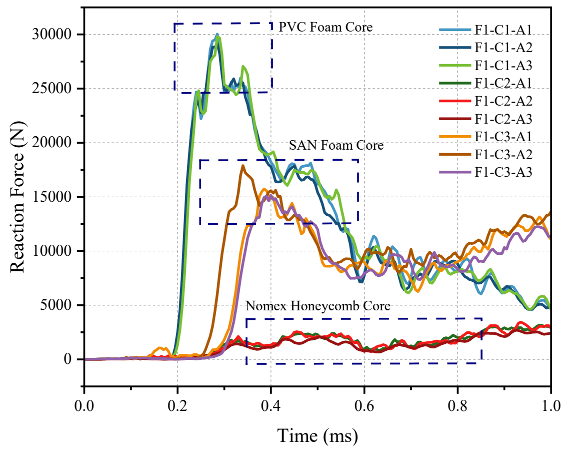

Figure 12. Time-history comparison of reaction forces based on core material (PVC foam, Nomex honeycomb, and SAN foam).

The graph shows that the reaction force values of the composite sandwich structure with a uniform material configuration are divided into three main clusters based on the type of core used. The PVC foam core produces the highest reaction force, reaching around 30,000 N, followed by SAN foam with reaction forces in the range of 17,500 N, while the honeycomb core shows the lowest reaction force, at only about 2,500 N.

Based on the reaction force data for each variation, the transmitted impulse through the sandwich panel can be determined, as shown in Fig. 13. For the sandwich structure with a PVC foam core and a uniform material configuration, Fig. 13a, the aramid facesheet exhibits the lowest transmitted impulse, at approximately 7,000 N·s, followed by basalt at 9,000 N·s. In comparison, the carbon facesheet produces the highest value of 10,500 N·s. This difference indicates that facesheets with higher stiffness tend to transmit greater impulse loads to the support, as they deform less and transfer more energy directly rather than dissipating it through internal mechanisms.

In the honeycomb core configuration, Fig. 13b, the analysis shows a similar trend, with the aramid facesheet consistently resulting in the lowest transmitted impulse, followed by basalt and carbon. Meanwhile, for the SAN foam core, Fig. 13c, the measured transmitted impulse values are not entirely uniform, but they still follow the same general trend, with a maximal value of approximately 8,000 N·s observed for the carbon facesheet combined with polyurethane adhesive.

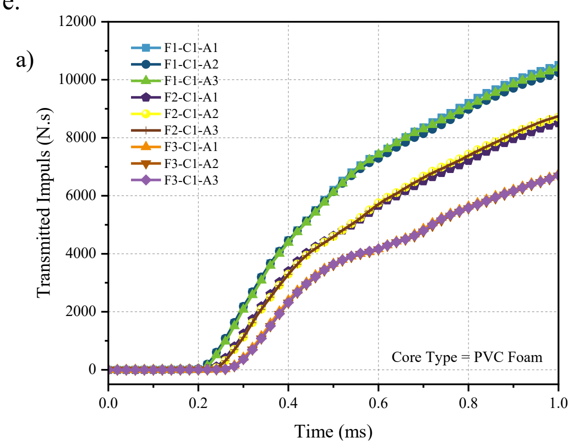

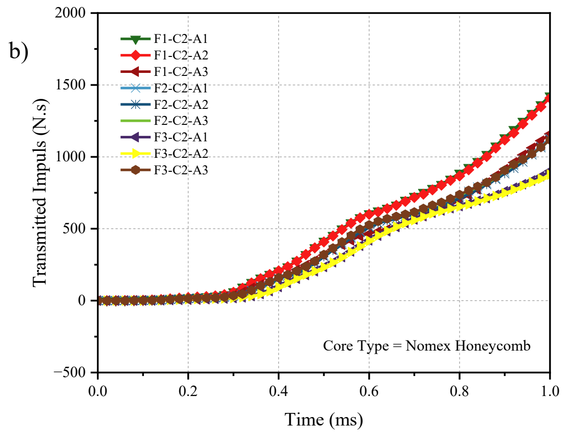

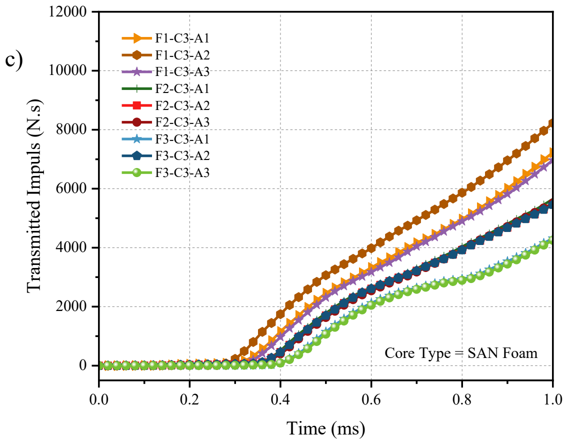

Figure 13. Transmitted impulse of the sandwich panel: a) PVC foam core; b) Nomex honeycomb core; c) SAN foam core.

In general, higher transmitted impulse values indicate a lower capability of the structure to dissipate impact energy, as most of the input energy is transmitted to the supports rather than being absorbed through deformation mechanisms and internal material damping. These observations suggest that while the core type primarily governs energy-absorption characteristics, the facesheet material also plays a significant role: a stiffer facesheet limits structural deformation but tends to transmit more energy to the support.

Absorbed energy

Absorbed energy represents the ability of a material to absorb energy from impulse loads. From the simulations with uniform cores, the carbon facesheet shows the highest absorbed energy (16,000 J), followed by aramid (14,000 J) with a polyurethane adhesive. In comparison, basalt shows the lowest (8,200 J), Fig. 14a.

The high stiffness of the carbon facesheet allows the structure to withstand large impulse energy, so more energy is absorbed through global panel deformation and core compression. The more compliant aramid facesheet absorbs less energy because panel deformation is limited, and the energy entering the structure is relatively low.

A similar trend is observed for the SAN foam core, Fig. 14b, where the carbon-SAN foam-polyurethane configuration achieves the highest energy absorption (22,000 J), while other variations fall within 10,000-16,000 J, comparable to the PVC foam core. The energy absorption curve of the PVC foam core is gentler than that of SAN foam, reflecting differences in deformation behaviour and energy dissipation mechanisms. PVC and SAN foam cores absorb more energy than honeycomb because local deformation and material compression dissipate part of the impulse energy. However, the total absorbed energy of foam cores remains limited because the main mechanism is local cell deformation or core compression rather than global panel deformation.

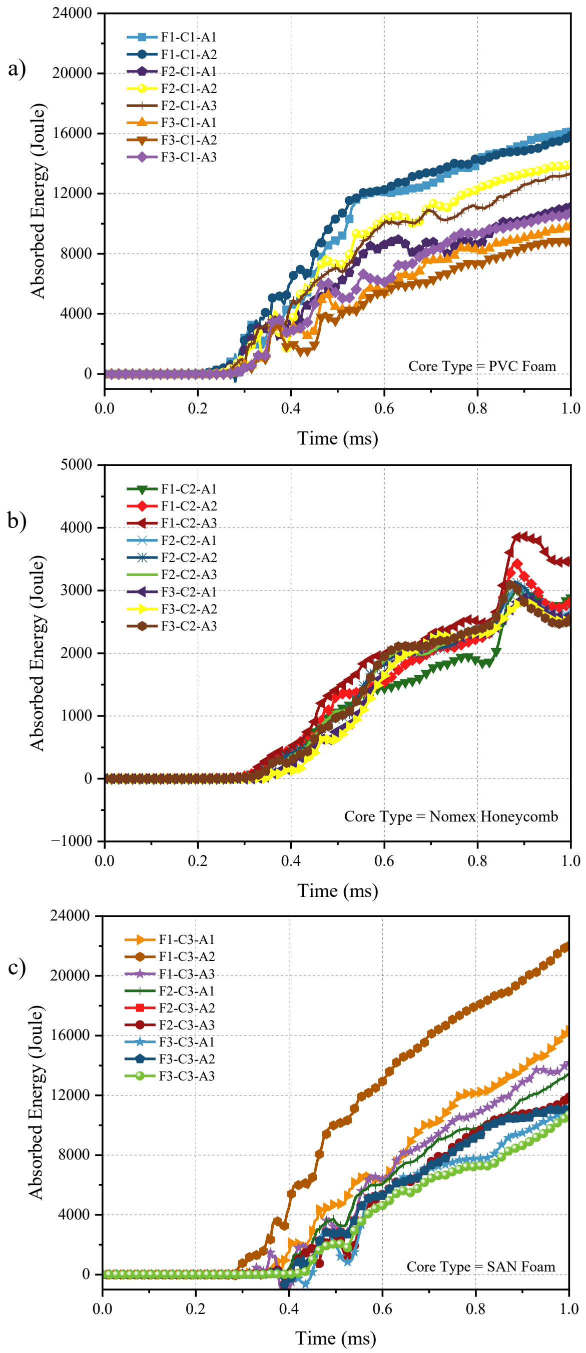

Figure 14. Absorbed energy of the sandwich panel: a) PVC foam core; b) Nomex honeycomb core; c) SAN foam core.

In contrast, the Nomex honeycomb core, Fig. 14c, exhibits low absorbed energy (4,000 J) and relatively uniform values across all configurations, resulting in the highest panel displacement. Although the honeycomb core effectively reduces the reaction force, its stiff cells limit internal deformation, thereby transmitting most of the energy to the supports.

CONCLUSIONS

This study shows that the combination of facesheet, core, and adhesive materials primarily governs the impulse response of sandwich panels. Carbon facesheet generally exhibits higher initial displacement than aramid and basalt, but with appropriate material pairing, they can achieve superior overall performance. In contrast, the more compliant aramid facesheet results in lower transmitted impulse and absorbed energy because less impulse energy enters the structure.

Regarding the core, PVC foam exhibits a small displacement (1.3 mm) and moderate absorbed energy (16 kJ) due to its balanced stiffness and effective local compression. SAN foam provides the highest absorbed energy (22 kJ) due to its greater compressive capacity, but it still transmits a moderate impulse (8 kN·s) because of significant core deformation. Conversely, the Nomex honeycomb core produces a low reaction force (3.5 kN) but limited absorbed energy (4 kJ), as loads are primarily carried by local deformation of stiff, thin-walled cells, which restricts internal energy dissipation and increases global panel displacement.

Adhesive material variations have a relatively minor effect compared to facesheet and core, although vinyl ester shows slightly better performance in limiting displacement under large core deformation. Overall, the results confirm that the impulse response of OWC sandwich panels is governed by the interplay among face-sheet deformation, core compression mechanisms, and material stiffness. These findings contribute to the design of OWC sandwich structures by guiding the selection of material combinations that enhance impulse energy absorption, reduce transmission of force to supports, and control panel displacement, thereby improving structural reliability.

However, factors such as moisture absorption, prolonged seawater exposure, and material ageing are beyond the scope of this work. Future research will address these aspects to provide a more comprehensive evaluation of the long-term durability and structural reliability of composite-based OWC.

ACKNOWLEDGEMENTS

This research is based on results from the Joint Research of Ocean Energy programme conducted with the Institute of Ocean Energy at Saga University. The authors would like to express their sincere appreciation to the Institute of Ocean Energy at Saga University for its support. This work was supported by the RKAT Universitas Sebelas Maret - Year 2026, under the Research Scheme of 'Penelitian Pascasarjana Magister (PPsM-UNS)', with research grant/contract no. 460/UN27.22/PT.01.03/2026. The authors highly acknowledge this support.

REFERENCES

1. Gielen, D., Boshell, F., Saygin, D., et al. (2019), *The role of renewable energy in the global energy transformation*, Energy Strateg. Rev. 24: 38-50. doi: 10.1016/j.esr.2019.01.006
2. Fauzi, F.N., Adiputra, R., Firdaus, N., Prabowo, A.R. (2024), *Comparative study of wave forces on a spar-type FOWT under free floating conditions: The role of slenderness*, In: Proc. of the 9th Conf. and Exhib. on Sustainable Energy and Adv. Mater.,

Springer Nature Singapore, pp.615-619. doi: 10.1007/978-981-97-0106-3_97
3. Fauzi, F.N., Puryantini, N., Prabowo, A.R., et al. (2024), *Implementation assessment of the offshore wind turbine (OWT) for remote regions' electrification in Indonesia based on geographical potential and economic attractiveness*, Eng. Sci. 32: 1295. doi: 10.30919/es1295
4. Falcão, A.F. de O. (2010), *Wave energy utilization: A review of the technologies*, Renew. Sustain. Energy Rev. 14(3): 899-918. doi: 10.1016/j.rser.2009.11.003
5. Muzaqih, A.F., Adiputra, R., Prabowo, A.R., et al. (2025), *Analysis of ultimate capacity of sandwich composite material against impulse load: A study case of fluid-structure interaction by FE approach*, Results Eng. 26: 105506. doi: 10.1016/j.rineng.2025.105506
6. Lenggana, B.W., Prabowo, A.R., Ubaidillah, U., et al. (2021), *Effects of mechanical vibration on designed steel-based plate geometries: behavioral estimation subjected to applied material classes using finite-element method*, Curved Layer. Struct. 8 (1): 225-240. doi: 10.1515/cls-2021-0021
7. Rasgianti, Adiputra, R., Nugraha, A.D., et al. (2024), *Design optimization of stiffening system for ocean thermal energy conversion (OTEC) cold water pipe (CWP)*, Results Eng. 23: 102863. doi: 10.1016/j.rineng.2024.102863
8. Krausz, T., Popa, C.F., Galațanu, S.V., Marșavina, L. (2023), *Numerical and experimental study for polycarbonate composites under static and dynamic tests*, Struct. Integr. Life, 23(3): 251-256.
9. Kautsar, H.A.A., Adiputra, R., Kusharjanta, B., et al. (2025), *Preliminary assessment of a novel OTEC CWP design using sand-filled sandwich pipe*, E3S Web Conf., The 5th Ed. of Oriental Days for the Environment ‘Green Lab. Solution for Sustainable Development’ (JOE5), 632: 03006. doi: 10.1051/e3sconf/202563203006
10. Nurcholis, A., Prabowo, A.R., Muhayat, N., et al. (2024), *Performances of the sandwich panel structures under fire accident due to hydrogen leaks: Consideration of structural design and environment factor using FE analysis*, Curved Layer. Struct. 11(1): 20240005. doi: 10.1515/cls-2024-0005
11. Afzali, M., Arani, A.G., Maraghi, Z.K. (2025), *Novel CFRP crash boxes with high absorption geometry reinforced with nano graphene oxide*, Struct. Integr. Life, 25(3): 445-451. doi: 10.69644/ivk-2025-03-0445
12. bin Mat Saad, K.A., bin Azman, A.K. (2020), *Optimization structure design of offshore oscillating water column (OWC) wave energy converte*r, In: C.L. Saw, T.K. Woo, S. Singh, et al. (Eds.) Advancement in Emerging Technologies and Engineering Applications. Lecture Notes in Mechanical Engineering. Springer Singapore, pp.163-173. doi: 10.1007/978-981-15-0002-2_18
13. Goeijenbier, B., Bricker, J., Antonini, A., et al. (2021), *Structural optimisation and behaviour of the breakwater integrated oscillating water column device. A combined 3D CFD and structural analysis*, J Coast. Hydr. Struct. 1: 1-22. doi: 10.48438/JCHS.2021.0002
14. Pan, S., Zhang, H., Geng, J., Zhao, X. (2025), *Hydrodynamic behavior of an offshore OWC power station under dam-break flows: Numerical and experimental study*, J Fluids Struct. 139: 104426. doi: 10.1016/j.jfluidstructs.2025.104426
15. Avachat, S., Qu, T., Zhou, M. (2018), *Geometry and size effects in response of composite structures subjected to water-based impulsive loading*, In: S. Gopalakrishnan, Y. Rajapakse (Eds.), Blast Mitigation Strategies in Marine Composite and Sandwich Structures. Springer Transactions in Civil and Environmental Eng. Springer Singapore, pp.443-470. doi: 10.1007/978-981-10-7170-6_23
16. Feng, H., Huang, W., Deng, S., et al. (2022), *Dynamic fluid-structure interaction of graded foam core sandwich plates to underwater blast*, Int. J Mech. Sci. 231: 107557. doi: 10.1016/j.ijmecsci.2022.107557
17. Wei, Z., Rong, J. (2025), *Dynamic response and damage mechanism of CFRP composite laminates subjected to underwater impulsive loading*, Appl. Sci. 15(20): 10888. doi: 10.3390/app152010888
18. He, X., Rong, J.L., Xiang, D.L. (2017), *Damage analysis of aluminium foam panel subjected to underwater shock loading*, Shock Vib. 2017(1): 6031414. doi: 10.1155/2017/6031414
19. Dahmane, M., Zahaf, S., Benkhettab, M., et al. (2021), *Application of the finite element method to vibration analysis of pipes conveying fluid flow*, Struct. Integr. Life, 21(1): 7-14.
20. Rasgianti, Muzaqih, A.F., Adiputra, R., et al. (2025), *Ultimate capacity of metal matrix composites sandwich under impulsive loads for marine structural applications*, Sustain. Mar. Struct. 7(4): 168-192. doi: 10.36956/sms.v7i4.2830
21. Prabowo, A.R., Ridwan, R., Braun, M., et al. (2023), *Comparative study of shell element formulations as NLFE parameters to forecast structural crashworthiness*, Curved Layer. Struct. 10(1): 20220217. doi:10.1515/cls-2022-0217
22. Nascimento, L.F.C., Louro, L.H.L., Monteiro, S.N., et al. (2018), *Limit speed analysis and absorbed energy in multilayer armor with epoxy composite reinforced with mallow fibers and mallow and jute hybrid fabric*, In: TMS Annual Meeting & Exhibition, Cham: Springer Int. Publ. pp.597-604. doi: 10.1007/978-3-319-72484-3_63
23. Mengal, A.N., Karuppanan, S., Wahab, A.A. (2014), *Structural analysis of basalt fiber reinforced plastic wind turbine blade*, In: MATEC Web Conf., EDP Sciences, 13: 04019. doi: 10.1051/matecconf/20141304019
24. Avachat, S., Zhou, M. (2015), *High-speed digital imaging and computational modeling of dynamic failure in composite structures subjected to underwater impulsive loads*, Int. J Impact Eng. 77: 147-165. doi: 10.1016/j.ijimpeng.2014.11.008
25. Zarrouk, T., Salhi, J.-E., Nouari, M., Barboucha, M. (2025), *Modeling of Nomex honeycomb structure milling assisted by longitudinal-torsional vibrations with a CZ10 combined tool: Optimization of tool wear and surface integrity*, Appl. Mech. 6(3): 47. doi: 10.3390/applmech6030047
26. Beznea, E.F., Baroiu, N., Chirica, I. (2021), *The static behavior of a ship deck panel made of composite materials*, Mater. Plast. 58(4): 147-157. doi: 10.37358/MP.21.4.5540
27. Banea, M.D., da Silva, L.F.M. (2009), *Adhesively bonded joints in composite materials: an overview*, Proc. Inst. Mech. Eng. Part L, J Mater.: Des. Appl. 223(1): 1-18. doi: 10.1243/14644207JMDA219

© 2026 The Author. Structural Integrity and Life, Published by DIVK (The Society for Structural Integrity and Life ‘Prof. Dr Stojan Sedmak’) (http://divk.inovacionicentar.rs/ivk/home.html). This is an open access article distributed under the terms and conditions of the Creative Commons Attribution-NonCommercial-NoDerivatives 4.0 International License